Time-reversal Invariant SU(2) Hofstadter Problem in Three Dimensional Lattices

Yi Li[1]

[1] *Princeton Center for Theoretical Science, Princeton University, Princeton, New Jersey 08544, USA*

(Dated: June 2, 2015)

We formulate the three-dimensional $SU(2)$ Landau level problem in cubic lattices with time-reversal invariance. By taking a Landau-type $SU(2)$ gauge, the system can be reduced into one-dimension, as characterized by the $SU(2)$ generalization of the usual Harper equations with a periodic spin-dependent gauge potential. The surface spectra indicate the spatial separation of helical states with opposite eigenvalues of a lattice helicity operator. The band topology is investigated from both the analysis of the boundary helical Fermi surfaces and the calculation of the $\mathbb{Z}_2$-index based on the bulk wave functions. The transition between a three-dimensional weak topological insulator to a strong one is studied as varying the anisotropy of hopping parameters.

PACS numbers: 73.43.Cd, 71.70.Ej, 75.70.Tj

arXiv:1410.6189v2 [cond-mat.str-el] 3 Jun 2015

I. INTRODUCTION

The study of topological states of matter has become a major research focus of contemporary condensed matter physics[1–3]. An early example is the two-dimensional (2D) quantum Hall effect based on the Landau level quantization of electrons in the magnetic field, whose topological band structure is characterized by the first Chern number[4–8]. Its chiral edge modes give rise to dissipationless charge transport and quantized Hall conductance. In the past decade, tremendous progress has been made on the time-reversal invariant topological insulators in both 2D and 3D, whose band structure topology is described by the $\mathbb{Z}_2$ index[9–15]. At the boundary, the 2D and 3D topological insulators exhibit 1D helical edge modes and 2D helical surface modes, respectively. Various systems of the 2D and 3D topological insulators have been observed experimentally through various spectroscopic and transport measurements[11,16–21]. Another important development is based on high-dimensional generalizations of Landau levels. Landau level wave functions explicitly exhibit elegant analytic properties, which played an important role in the study of 2D fractional quantum Hall effects[22,23]. Zhang and Hu[24] pioneered the study of Landau levels on four- and higher-dimensional spheres and other compact manifolds by coupling fermions to gauge potentials of non-Abelian monopoles[25–31].

Recently, Landau levels (LLs) in three- and higher dimensional flat continuum space have also been discussed[32–34]. In 3D and 4D, their Hamiltonians describe spin-$\frac{1}{2}$ fermions in an SU(2) gauge potential, which were constructed from harmonic oscillators with certain spin-orbit coupling (SOC). The corresponding Landau level wave functions are the same as those of harmonic oscillators, but they are reorganized by the SOC term to exhibit non-trivial topology. In the symmetric-type $SU(2)$ gauge, the 3D and 4D rotational symmetries are explicitly maintained with exactly flat energy spectra and degenerate angular momenta. The lowest Landau level wave functions exhibit interesting quaternion analyticity[32]. In the Landau-type gauge, they behave like spatially separated 2D helical Dirac fermion modes or 3D chiral Weyl fermion modes. Modes with opposite helicities or chiralities are shifted along the third or fourth dimension in opposite directions, respectively[33]. These LLs have also been generalized to high dimensional Dirac fermions and parity-breaking systems[35,36]. One issue of the topological states based on high-dimensional Landau levels is how to define their topological index. The non-trivial topology of filled Landau levels was illustrated through the effective boundary Hamiltonians, which exhibit helical Fermi surfaces[32,33,35]. However, unlike the 2D case, there was no full translation symmetry for the 3D Landau level Hamiltonians, and thus the $\mathbb{Z}_2$-index defined based on the Bloch wave function structure could not be applied.

A lattice construction of the Hofstadter Hamiltonian for the 3D LL problem will be helpful to directly calculate the topological index of that system with translation symmetry imposed. For the 2D case, the lattice version of the LL problem based on the $U(1)$ vector field is well known as the Hofstadter problem[37]. In the Landau gauge, the $U(1)$ vector potential becomes a periodic scalar potential in the reduced 1D Harper equation. The non-trivial Chern number is interpreted as the linking number between fundamental loops on the complexified energy surface with the topology of a Riemann surface[38,39]. Recently, this Hofstadter Hamiltonian was realized experimentally in optical lattices by laser-assisted tunneling[40–43]. Also, Hofstadter problems have been theoretically generalized to systems with non-Abelian gauge groups[44–46].

In this article, we will consider the 3D LLs of the Landau-type SU(2) gauge in which the system shows translation symmetry in the xy plane. For each pair of in plane momenta (k_x, k_y), the system can be reduced to one dimension, as described by the SU(2) Harper equation exhibiting the periodic configuration of spin-dependent potential. The bulk and surface spectra are explicitly calculated, and the non-trivial band topology are analyzed through the surface helical Fermi surface and also from the analysis on the parity eigenvalues of the bulk wave functions. Topological band structure transitions

between the weak and strong 3D topological insulators are studied.

The rest of this paper is organized as follows: In Sect. II, the lattice model for 3D LLs in the SU(2) Landau gauge and the corresponding SU(2) Harper equation are constructed. In Sect. III, the topological band structure is analyzed through the helical surface spectra and the $\mathbb{Z}_2$-index based on the parity eigenvalue analysis on the bulk wave function. In Sect. IV, the topological band structure transition in studied. Discussions on the relationship with the previous work on the 3D Hofstadter problem in the tilted magnetic field and experimental realizations are presented in Sect. V. Conclusions are summarized in Sect. VI.

II. 3D LANDAU LEVELS ON A CUBIC LATTICE AND THE 1D $SU(2)$ HARPER EQUATION

In this section, we construct the 3D $SU(2)$ Landau level in lattices with full three-dimensional translation symmetry, and we show that it can be reduced into a family of generalized 1D $SU(2)$ Harper equations.

A. The 3D Landau level in the continuum

The 2D Landau level in the magnetic field has been generalized into 3D continuum, which was defined as a spin-$\frac{1}{2}$ electron coupling to an external SU(2) vector potential $\vec{A}$ and a scalar potential $V(x)$[32,33] as

$$H_{3DLL} = \frac{(\vec{p} - \frac{e}{c}\vec{A}(\vec{r}))^2}{2m} + V(\vec{r}). \quad (1)$$

In the Landau-type gauge, $\vec{A}(\vec{r})$ and $V(\vec{r})$ only depend on the z-coordinate, which can be chosen as

$$A_x(\vec{r}) = G\sigma_y z, \quad A_y(\vec{r}) = -G\sigma_x z, \quad A_z = 0;$$
$$V(\vec{r}) = -\frac{1}{2}m\omega^2 z^2, \quad (2)$$

where G is a coupling constant, $\sigma_{x,y,z}$ are Pauli matrices, and $\omega = eG/(mc)$. Equation (1) describes a 3D topological insulator possessing the TR symmetry and translational symmetry along the x-y plane. At an open boundary perpendicular to the z axis, each filled Landau level contributes a helical Dirac Fermi surface[32]. The surface states carrying opposite helicities are spatially separated at $z > 0$ and $z < 0$ surfaces respectively. This can be shown explicitly by expanding Eq. (1) as $H_{3DLL} = p_z^2/(2m) + 1/2m\omega^2[z - l_{so}^2 k_{2d}\hat{\Sigma}_{2d}(\hat{k}_{2d})]^2$, where $\vec{k}_{2d} = (k_x, k_y)$ and $\hat{\Sigma}_{2d}$ is the helicity operator defined as $\hat{\Sigma}_{2d}(\hat{k}_{2d}) = \hat{k}_x\sigma_y - \hat{k}_y\sigma_x$ with $\hat{k}_{x,y} = k_{x,y}/k_{2d}$. Alternatively, Eq. (1) is also equivalent to an electron in a quantum-well with z-dependent spin-orbit coupling strength as

$$H_{3DLL} = \frac{\vec{p}^2}{2m} + \frac{1}{2}m\omega^2 z^2 - \omega z(p_x\sigma_y - p_y\sigma_x). \quad (3)$$

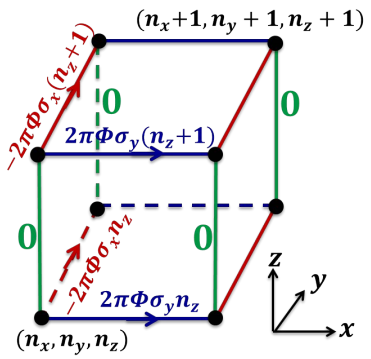

FIG. 1. (Color online) The configuration of Landau-type $SU(2)$ gauge fields $\vec{A}(n_x, n_y, n_z)$ defined on the bonds of the cubic lattice, which has coordinate dependence only on n_z.

B. The SU(2) Hofstadter problem in the 3D cubic lattice

Now let us construct the lattice version of the 3D LL Hamiltonian Eq. (1), or, Eq. (3) as a tight-binding model on a cubic lattice. The kinetic energy becomes the nearest-neighbor hopping term; the SO coupling is realized as the $SU(2)$ gauge potential defined on each bond of the cubic lattice, and the scalar quadratic potential is converted as a periodic potential along the z axis on the lattice. The lattice Hamiltonian reads

$$H_{latt} = -\sum_{a,\vec{n},s,s'} t_a \Big\{ c^\dagger_{\vec{n}+\hat{e}_a,s}[e^{iA_{\vec{n}+\hat{e}_a,\vec{n}}}]_{ss'} c_{\vec{n},s'} + h.c. \Big\} + \sum_{\vec{n},s} V(n) c^\dagger_{\vec{n},s} c_{\vec{n},s}, \quad (4)$$

where $c_{\vec{n},s}$ ($c^\dagger_{\vec{n},s}$) is the annihilation (creation) operator of electrons at site $\vec{n} = (n_x, n_y, n_z)$ with spin $s = \uparrow, \downarrow$. $\hat{e}_a$ and t_a ($a = x, y, z$) are, respectively, the lattice unit vector and the hopping amplitude along the a-direction. The previous $SU(2)$ Landau-type gauge of Eq. (2) defined in the continuum can now be defined on each bond of the cubic lattice as follows:

$$A_{\vec{n}+\hat{x},\vec{n}} = \frac{2\pi\Phi}{\Phi_0}\sigma_y n_z, \quad A_{\vec{n}+\hat{y},\vec{n}} = -\frac{2\pi\Phi}{\Phi_0}\sigma_x n_z,$$
$$A_{\vec{n}+\hat{z},\vec{n}} = 0, \quad (5)$$

where $\Phi_0 = e/(hc)$ is the flux quantum, whose value is taken as 1 in this paper. As illustrated in Fig. 1, this gauge configuration can be obtained by rotating a 2D quantum spin-Hall (QSH)[47] Hofstadter problem defined in the xz plane by 90° around its z axis, so that its yz plane forms another QSH problem. The QSH problem at each plane can be understood as two Kramerss copies of the 2D U(1) Hofstadter problem with opposite fluxes for opposite spins. Further, because of the SOC, the spin quantization axis along y in the xz plane QSH problem is also rotated by 90°, to be along x, in the yz plane QSH

problem, which imposes the 3D feature of the topological insulator and reflects the four-fold SO coupled rotation symmetry in the lattice. For later convenience, we choose the n_z-dependent scalar potential as

$$V(n_z) = 2t_y \cos(2\pi \frac{\Phi}{\Phi_0} n_z). \quad (6)$$

$A_{\vec{n}+\hat{e}_a,\vec{n}}$ and $V(n_z)$ are independent of n_x and n_y, hence, Eq. (4) explicitly maintains translational symmetry along the xy plane. In addition, it also possesses time-reversal and parity symmetries.

Next we transform the lattice Hamiltonian Eq. (4) into the 1D Harper equation. Because of the translation symmetry in the xy plane, the in plane momenta k_x and k_y are good quantum numbers. For a given set of values of k_x and k_y, we introduce the partial Fourier transform as

$$c^\dagger_{n_z,s}(k_x,k_y) = \frac{1}{\sqrt{L_x L_y}} \sum_{n_x,n_y} e^{-ik_x n_x - ik_y n_y} c^\dagger_{\vec{n},s}. \quad (7)$$

Then Eq. 4 is reduced to

$$\begin{aligned} H_z(k_x,k_y) = &-t_z \sum_{n_z;s} \Big\{ c^\dagger_{n_z+1;s}(k_x,k_y) c_{n_z;s}(k_x,k_y) + h.c. \Big\} \\ &- 2 \sum_{n_z,s,s'} c^\dagger_{n_z;s}(k_x,k_y) V_{n_z;s,s'} c_{n_z;s'}(k_x,k_y) \end{aligned} \quad (8)$$

in which

$$\begin{aligned} V_{n_z;s,s'} = &\delta_{ss'} r(k_x,k_y) \cos(2\pi n_z \frac{\Phi}{\Phi_0}) \\ &+ [-i\tilde{k}_- \sigma_+ + i\tilde{k}_+ \sigma_-]_{ss'} \sin(2\pi n_z \frac{\Phi}{\Phi_0}), \end{aligned} \quad (9)$$

and

$$\begin{aligned} r(k_x,k_y) &= t_x \cos k_x + t_y(\cos k_y - 1), \\ \tilde{k}_\pm &= t_x \sin k_x \pm i t_y \sin k_y, \\ \sigma_\pm &= \frac{1}{2}(\sigma_x \pm i\sigma_y). \end{aligned} \quad (10)$$

Eq. (8) consists of the usual hopping along the z-direction and the periodic onsite spin-dependent potential Eq. (9). In comparison, the Harper equation for the 2D Landau level problem in the Landau gauge is a hopping Hamiltonian in the presence of a periodic onsite scalar potential. As a result, Eq. (8) maintains time-reversal symmetry as

$$H_z(k_x,k_y) = T H_z(-k_x,-k_y) T^{-1} \quad (11)$$

with $T = i\sigma_2 K$ and K is the complex conjugation.

C. The SU(2) transfer matrix

We consider the case of $\Phi/\Phi_0 = p/q$ with p and q coprime integers, and then $H_z(k_x,k_y)$ becomes periodical along the z-direction with an enlarged unit cell size of q. Below we also assume that the lattice size along the z-direction L_z is an integer multiple of q as $L_z = lq$. On a single particle basis with momenta k_x and k_y,

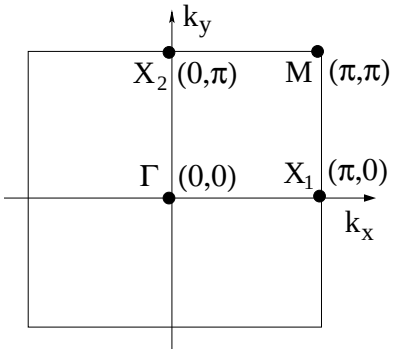

FIG. 2. The 2D surface Brillouin zone and the time-reversal invaraint points $\Gamma = (0,0)$, $X_1 = (\pi,0)$, $X_2 = (0,\pi)$, and $M = (\pi,\pi)$.

$$|\Psi(k_x,k_y)\rangle = \sum_{n_z;s} \Psi_{n_z;s}(k_x,k_y) c^\dagger_{n_z;s}(k_x,k_y)|0\rangle, \quad (12)$$

the corresponding Harper equation becomes

$$\begin{aligned} &-[\Psi_{n_z+1;s}(k_x,k_y) + \Psi_{n_z-1;s}(k_x,k_y)] \\ &-\frac{2}{t_z} \sum_{s'} V_{n_z;s,s'} \Psi_{n_z;s'}(k_x,k_y) = \epsilon \Psi_{n_z;s}(k_x,k_y), \end{aligned} \quad (13)$$

where $\epsilon = E/t_z$. In the form of transfer matrix, Eq. (13) is represented as

$$\begin{aligned} \begin{bmatrix} \Psi_{n_z+1,s}(\epsilon,k_x,k_y) \\ \Psi_{n_z,s}(\epsilon,k_x,k_y) \end{bmatrix} &= T_{n_z;ss'}(\epsilon,k_x,k_y) \\ &\times \begin{bmatrix} \Psi_{n_z,s'}(\epsilon,k_x,k_y) \\ \Psi_{n_z-1,s'}(\epsilon,k_x,k_y) \end{bmatrix}. \end{aligned} \quad (14)$$

The transfer matrix is defined as

$$T_{n_z;ss'}(\epsilon,k_x,k_y) = \begin{pmatrix} \mathcal{E}_{ss'} & -I_{ss'} \\ I_{ss'} & 0 \end{pmatrix}, \quad (15)$$

in which I is the 2×2 identity matrix; and

$$\begin{aligned} \mathcal{E} = &-\epsilon I - \frac{2}{t_z} r(k_x,k_y) \cos(2\pi\Phi n_z) \\ &- \frac{2}{t_z} \sin(2\pi\Phi n_z)(-i\tilde{k}_- \sigma_+ + i\tilde{k}_+ \sigma_-). \end{aligned} \quad (16)$$

Noticing that the spin-dependence of the transfer matrix $T_{n_z;ss'}$ is n_z-independent, thus the Harper equation (Eq. (13)) can be decoupled into two sets in the "lattice helicty" eigen-basis. The lattice helicty operator is defined as

$$\Sigma_{\rm L} = t_x \sin k_x \sigma_y - t_y \sin k_y \sigma_x, \quad (17)$$

which can be viewed as the lattice generalization of the helicity operator $\Sigma = \hat{k}_x \sigma_y - \hat{k}_y \sigma_x$ in the continuum. Its

eigenvalues are $\pm\sqrt{t_x^2\sin^2 k_x + t_y^2 \sin^2 k_y}$, corresponding to the in plane eigenstates

$$\chi_\pm(k_x,k_y) = \frac{1}{\sqrt{2}}\begin{pmatrix} \mp i\frac{t_x \sin k_x - i t_y \sin k_y}{\sqrt{t_x^2\sin^2 k_x + t_y^2\sin^2 k_y}} \\ 1 \end{pmatrix}. \quad (18)$$

Under the time-reversal transformation, Σ_L as well as its eigenstates are invariant. In this representation, the transfer matrix $T_{n_z;ss'}$ is decomposed into two sets of $T_{n_z;\pm}$ with the 2×2 form for Σ_L positive and negative helicities, respectively, as

$$T_{n_z;\pm}(\epsilon,k_x,k_y) = \begin{pmatrix} \mathcal{E}_\pm & -1 \\ 1 & 0 \end{pmatrix}, \quad (19)$$

with

$$\mathcal{E}_\pm = -\epsilon - \frac{2}{t_z} r(k_x,k_y)\cos(2\pi\Phi n_z) \mp \frac{2}{t_z}\sin(2\pi\Phi n_z)\sqrt{t_x^2\sin k_x^2 + t_y^2 \sin k_y^2}. \quad (20)$$

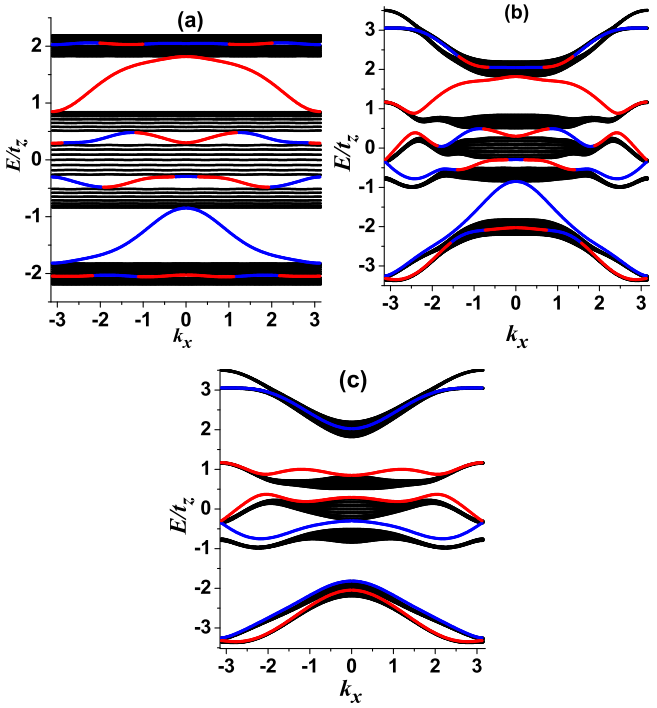

FIG. 3. The bulk and surface spectra along the high symmetry lines connecting time-reversal invariant points in the Brillouin zone. (a) X_1-Γ-X_1, (b) M-Γ-M, (c) M-X_2-M, respectively. The red and blue lines represent the surface states with positive and negative helicities, respectively. Here, only surface modes localized at the lower boundary are plotted, and those of the upper surface are of the same values in the energy spectrum but with opposite lattice helicities. The following parameters are used: $t_x = t_y = 0.5$, $t_z = 1$, $p/q = 2/7$, and $L_z = 56$.

Following the method introduced in Ref. [39], we define the matrix $M^\pm(\epsilon,k_x,k_y)$ as the product of $T_{i;\pm}(\epsilon,k_x,k_y)$ for sites i's in a unit cell with q-sites as

$$M^\pm(\epsilon,k_x,k_y) = \prod_{i=1}^{q} T_{i;\pm}(\epsilon,k_x,k_y). \quad (21)$$

For the open boundary condition, the energy of the surface states can be determined by the zeros of the matrix elements $M_{21}^\pm(\epsilon,k_x,k_y)$ which are the roots of $(q-1)$th-order polynomial equations. For each lattice helicity sector, the $q-1$ roots $\mu_j^\pm (j = 1,2,..,q-1)$ denote the surface states in the $q-1$ gaps between adjacent bands.

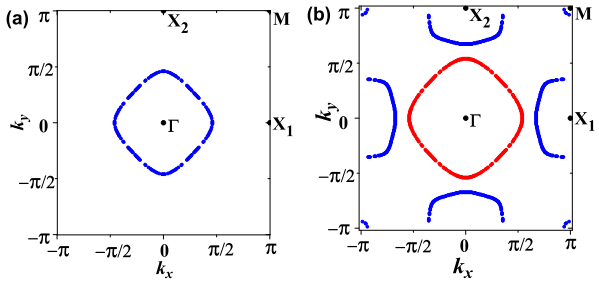

FIG. 4. (Color online) The boundary Fermi surface for states localized at the lower surface. Here, blue and red colors represent the negative and positive helicity states respectively. (a) $E_F = -1.5t_\parallel$ lying in the 2nd gap. Only one boundary helical Fermi surface appears. (b) $E_F = -0.47t_\parallel$ lying the 3rd gap. There are four boundary helical Fermi surfaces. Parameter values are $t_x = t_y = 0.5$, $t_z = 1$, $p/q = 2/7$, and $L_z = 56$.

III. THE BAND TOPOLOGY WITH THE TETRAGONAL SYMMETRY

In this section, we present the numeric results of the surface and bulk energy spectra of the 3D Hofstadter problem, as well as the analysis of Z_2 topological index from the parity eigenvalues of the bulk wave functions. We first consider the case with tetragonal symmetry in the xy plane.

A. The energy spectra

The Harper equation (Eq. (8)) is solved numerically with respect to k_x and k_y in the 2D Brillouin zone as depicted in Fig. 2. A typical flux value of $\Phi = p/q = 2/7$ is used: Each unit cell contains 7 sites, thus the spectra consist of 7 bands. To fully open band gaps, we choose an anisotropic ratio between t_z and $t_{x,y}$ as $t_x/t_z = t_y/t_z = 0.5$. The bulk and surface spectra are plotted along different high symmetry lines connecting time-reversal invariant points in the Brillouin zone in Fig. 3 (a), (b), and (c), respectively. In each gap between adjacent bands, helical surface states appear with their helicities marked with different colors in Fig. 3.

The states on the upper and lower surfaces can be distinguished by the values of $M_{11}^{\pm}(\epsilon)$ where the ϵ is a surface state energy. If $|M_{11}^{\pm}(\mu_j)| < 1$ (> 1), then the corresponding eigenstates are localized on the lower ($n_z = 1$) or upper ($n_z = L_z$) boundaries, respectively[39]. If $|M_{11}^{\pm}(\mu_j)| = 1$, it means that the corresponding states merge into bulk states, and they are no longer considered surface states. Because of parity symmetry, the upper surface spectrum with momenta (k_x, k_y) should be the same as that of the lower surface with $(-k_x, -k_y)$. Further, since the spin polarization is invariant under inversion operation, the corresponding surface states on the upper and lower surfaces are of opposite lattice helicity eigenvalues, thus only the surface states on the lower surface are depicted in Fig. 3.

The spectra are plotted in Fig. 3 along the high symmetry lines connecting time-reversal invariant points in the Brillouin zone. In Fig. 3 (a), the spectra are presented along the cut of X_1-Γ-X_1. The Harper equation (Eq. (13)) along this cut is the same as that of the 2D Hofstadter problem in the magnetic field[39] but with Kramers doubling because of the time-reversal symmetry. As a result, the surface modes appear in terms of Kramers doublet pairs. For the band gap 1 to 6 counted from bottom to top, along the cut of X_1-Γ-X_1, here are 3, 1, 2, 2, 1, and 3 branches of Kramers doublets across the gap, respectively. This pattern remains the same as along the cut from M-Γ-M shown in Fig. 3 (b). Along the path M-X_1-M, the surface states do not run across the band gap.

(k_x, k_y, k_z)	B_1	B_2	B_3	B_4	B_5	B_6	B_7
$(0,0,0)$	+	+	−	−	+	+	−
$(0,0,\pi)$	+	−	+	−	+	−	+
$(0,\pi,0)$	+	−	+	−	+	−	+
$(0,\pi,\pi)$	−	+	+	−	−	+	+
$(\pi,0,0)$	+	−	+	−	+	−	+
$(\pi,0,\pi)$	−	+	+	−	−	+	+
$(\pi,\pi,0)$	+	−	+	−	+	−	+
(π,π,π)	−	+	+	−	−	+	+
$\prod_{a=1}^{8}\xi_a^i$	−	+	−	+	−	+	−
$\mathbb{Z}_2$	o	o	e	e	o	o	

TABLE I. The parity eigenvalues ξ_a^i of the 3D bulk states at eight time-reversal invariant states. $B_i (i = 1 \sim 7)$ represents the i-th band counted from bottom to top, and $a = 1 \sim 8$ is the index of states at the 8 time-reversal invariant momenta. The $\mathbb{Z}_2$ index e or o at the column of B_i represents that the system is $\mathbb{Z}_2$-trivial or non-trivial when the lowest i bands are filled. The parameter values are $t_x = t_y = 0.5$, $t_z = 1$, and $p/q = 2/7$.

B. Boundary Fermi surface and the $\mathbb{Z}_2$-index

To have a global view of the surface spectra, we present the Fermi surfaces of states localized at the lower boundary of the system. The Fermi energies lying between bands 2 and 3, and between bands 3 and 4 are shown in Fig. 4 (a) and (b), respectively. In the former case, there is only one Fermi circle enclosing the Γ point, which is helical according to the operator Σ_L, and thus if bands 1 and 2 are filled, the system is $\mathbb{Z}_2$ topological non-trivial. In this case, the boundary Fermi surface can be viewed as a consequence of a rotation of the edge Fermi points of the 2D QSH states in the xz plane. This is a strong 3D topological insulator, which means for boundaries along the xz and yz-directions, there should also exist odd numbers of helical Fermi surfaces.

On the other hand, if the Fermi energy lies between bands 3 and 4, there is one Fermi surface around each time-reversal invariant point Γ, two M's, and R, respectively. Three of them are of the same helicity, and the other one is of the opposite helicity. For the case with bands 1, 2, and 3 filled, the system becomes $\mathbb{Z}_2$ trivial. We have also checked the cases in which the Fermi energy is lying in the gap between bands 4 and 5, and between 5 and 6. The topology of the helical boundary Fermi surfaces is very similar to that depicted in Fig. 4 (a) and (b), respectively, but the helicity patterns are opposite. Because bands 1 and 2 overlap, there does not exist a full direct gap over the entire Brillouin zone. The boundary Fermi surfaces are not plotted for the Fermi energy lying in this regime.

The lattice Hamiltonian of Eq. (4) conveniently enables the periodicity in the z-direction, so that we can quantitatively calculate its $\mathbb{Z}_2$-index. Further, because of the inversion symmetry, the $\mathbb{Z}_2$-index is conveniently calculated by examining the parity eigenvalues of the bulk states at time-reversal invariant lattice momenta[13]. There are eight such lattice momenta (k_x, k_y, k_z) with $k_{x,y} = 0$ or π, and $k_z = 0$ or $\frac{\pi}{q}$. The wave functions in each band at these momenta are parity eigenstates and the associated eigenvalues ξ_i^a are presented in Table I, where $a = 1 \sim 8$ is the momentum index and $i = 1 \sim 7$ is the band index. For the case that the lowest i bands are all filled, the $\mathbb{Z}_2$ index equals $\prod_{j=1}^{i}\prod_{a=1}^{8}\xi_i^a$, which is presented in Table I. It shows that when the Fermi energy lies in the 1st, 2nd, 5th and 6th gaps, the system is $\mathbb{Z}_2$ non-trivial. On the other hand, if the Fermi energy lies in the 3rd and the 4th gaps, the system is $\mathbb{Z}_2$ trivial, where the three weak $\mathbb{Z}_2$ indices are also trivial. These results obtained from parity eigenvalues of bulk wave functions are consistent with that obtained from analyzing boundary helical Fermi surfaces in Fig. 4.

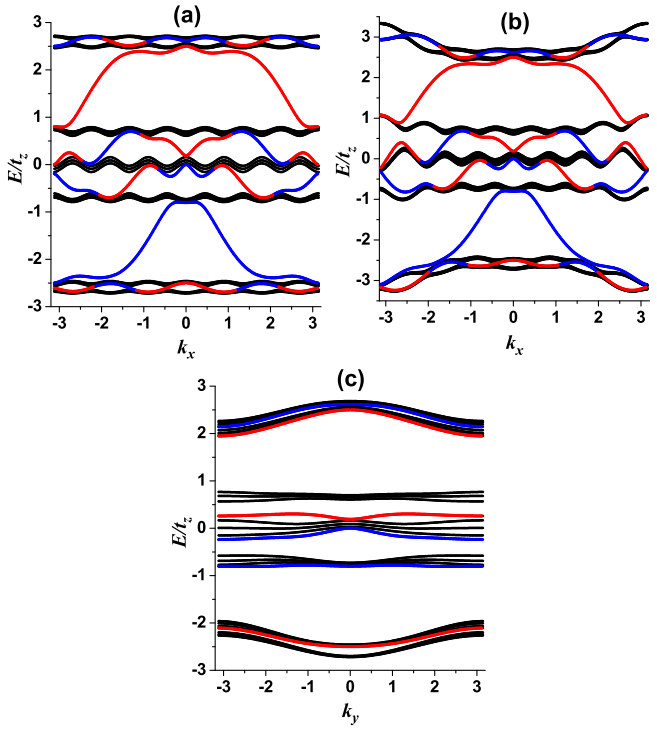

FIG. 5. The bulk and surface spectra along the time-reversal invariant paths of (a) X_1-Γ-X_1, (b) M-Γ-M, $(c)$$X_2$-Γ-$X_2$, respectively. The red and blue lines represent helical modes on the lower boundary with positive and negative helicities, respectively. The following parameters are used: $t_x = t_z = 1$, $t_y = 0.2$, $p/q = 2/7$, and $L_z = 56$.

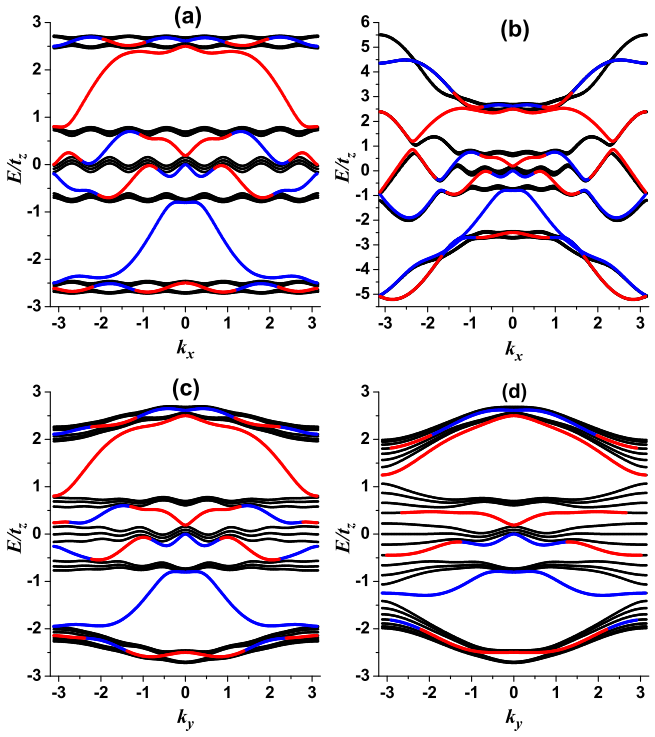

FIG. 6. The bulk and surface spectra along the time-reversal invariant paths. (a) X_1-Γ-X_1, (b) M-Γ-M, $(c)$$X_2$-Γ-$X_2$ for $t_x = t_z = 1$ and $t_y = 0.8$; $(d)$$X_2$-Γ-$X_2$ for $t_x = t_z = 1$ and $t_y = 0.5$. The red and blue lines represent helical modes on the lower boundary with positive and negative helicities, respectively. The following parameters are used:$p/q = 2/7$, and $L_z = 28$.

IV. TRANSITION FROM WEAK TO STRONG TOPOLOGICAL INSULATING STATES

In this section, we consider the crossover of the Hofstadter problem from the quasi-2D quantum spin Hall class to the 3D topological insulator class, i.e, the transition between weak and strong $\mathbb{Z}_2$-classes.

Now, let us set $t_x = t_z = 1$ but tune t_y from small values to 1. In the case of $t_y = 0$, Eq. 4 becomes decoupled xz-layers. Each xz-layer is the Kramers doubling of the 2D Hofstadter problem with spin polarized along the $\pm y$-direction. As t_y increases, energy dispersion develops along the y-direction and the direction of spin polarization also twists. However, the band topology remains the same at small values of t_y. In Fig. 5 (a), (b), and (c), the bulk and surface spectra at $t_y = 0.2$ are presented along the cuts of X_1-Γ-X_1, M-Γ-M, and X_2-Γ-X_2, respectively. Along X_1-Γ-X_1 and M-Γ-M, the bulk and surface spectra are qualitatively the same as those in Fig. 3 (a) and (b), respectively. The numbers of branches of Kramers doubles are $3, 1, 2, 2, 1, 3$, respectively, for the i-th band gap with $i = 1 \sim 6$. However, the xy plane is highly anisotropic. Along the cut of k_y axis, i.e., X_2-Γ-X_2, the spectra show no non-trivial mid-gap boundary modes across all gaps. In other words, this anisotropic case is a 3D weak topological insulator, which is topolog-

(k_x, k_y, k_z)	B_1	B_2	B_3	B_4	B_5	B_6	B_7
$(0,0,0)$	+	+	−	−	+	+	−
$(0,0,\pi)$	+	−	+	−	+	−	+
$(0,\pi,0)$	+	+	−	−	+	+	−
$(0,\pi,\pi)$	+	−	+	−	+	−	+
$(\pi,0,0)$	+	−	+	−	+	−	+
$(\pi,0,\pi)$	−	+	+	−	−	+	+
$(\pi,\pi,0)$	+	−	+	−	+	−	+
(π,π,π)	−	+	+	−	−	+	+
$\prod_{a=1}^{8}\xi_a^i$	+	+	+	+	+	+	+
$\mathbb{Z}_2$	e	e	e	e	e	e	
$\mathbb{Z}_{2,xz}$	o	o	e	e	o	o	
$\mathbb{Z}_{2,yz}$	e	e	e	e	e	e	
$\mathbb{Z}_{2,xy}$	e	e	e	e	e	e	

TABLE II. The parity eigenvalues ξ_a^i of the 3D bulk states at eight time-reversal invariant states and values of the $\mathbb{Z}_2$ index. Although the values of the strong $\mathbb{Z}_2$ index are all trivial, those of the weak $\mathbb{Z}_2$ index can be non-trivial in the xz-direction. Parameter values are $t_x = t_z = 1$, $t_y = 0.2$, and $p/q = 2/7$.

ically non-trivial only along the xz plane.

This result can be confirmed from the calculation of the bulk $\mathbb{Z}_2$-index. Similarly to Table I, in Table II, we also present the corresponding parity eigenvalues ξ_i^a for bulk wave functions at eight time-reversal invariant momenta ($a = 1 \sim 8$) of bands i ($i = 1 \sim 7$). The values of the strong $\mathbb{Z}_2$-index are all trivial for all the band gaps. Nevertheless, the weak $\mathbb{Z}_2$-index in the xz-direction exhibits a non-trivial pattern, which is non-trivial for the i-th band gap with $i = 1, 2, 5$ and 6, and thus is consistent with the evenness of the branches of boundary Kramers doublets presented in Fig. 5 (a). The weak $\mathbb{Z}_2$ indices for the xy and yz-directions are all trivial. Therefore, at $t_y = 0.2$, the system is qualitatively stacked by a 2D-like topological insulator in the xz plane, and it forms a 3D weak topological insulator.

Now let us study the case with a large value of $t_y = 0.8$. The bulk and boundary spectra are plotted in Fig. 6 (a), (b) and (c) along the same cuts as taken in Fig. 5. In particular, along the y-direction cut X_2-Γ-X_2 in Fig. 6 (c), non-trivial boundary modes appear across the band gap, which exhibit a pattern similar to the spectra along the x-direction cut X_1-Γ-X_1. Although small anisotropy remains in the xy plane, the system has already become a 3D strong topological insulator. We have also calculated the parity eigenvalues of bulk wave functions at time-reversal invariant momenta, and the results are the same as that in Table I, which also indicates that the strong $\mathbb{Z}_2$ index is non-trivial.

The transition between weak and strong topological insulating states as t_y varies must involve bulk band closing. It can be found that the transition point occurs at $t_y = 0.5$. In this case, the periodic spin-dependent potential characterizing the Hofstadter problem $V_{n_z;ss'}$ defined in Eq. (9) vanishes at $\vec{k}_{2D} = (0, \pi)$. As shown in Fig. 6 (d), all the band gaps closes at $(0, \pi)$, which triggers this band topology transition.

V. DISCUSSIONS

The above study of SU(2) Hofstadter problems in three-dimensions differs fundamentally from previously studied 3D Hofstadter problems under a tilted magnetic field[48–52]. Firstly, the latter problem is U(1) in nature. There is only one fermion component on each lattice site; the phase on each link and the flux penetrating each plaquette are U(1). However, our case is a 3D non-Abelian SU(2) problem. Here, the spin-1/2 spinor is located on each lattice site, and the gauge potentials defined on links are noncommutative SU(2) phases. Secondly, the bulk topological classes and surface spectra of these two problems are fundamentally different. Our SU(2) case maintains time-reversal symmetry, and hence it belongs to the AII class characterized by the $\mathbb{Z}_2$-indices calculated above[53]. When the strong $\mathbb{Z}_2$-index is odd, it is a strong 3D $\mathbb{Z}_2$ topological insulator, and the surface spectra exhibit an odd number of Dirac cones as shown in Fig. 4. In contrast, the 3D U(1) problem breaks time-reversal symmetry, and it is not a genuinely novel topological class. Roughly speaking, it belongs to the AI class and can be understood the same as stacking layers of 2D quantum Hall systems. In other words, it is a weak 3D topological state inheriting 2D features. The boundary Fermi surfaces do not close form Dirac cones but rather disconnect forming Fermi arcs. Finally, the reduced 1D Hofstadter equations are also different in these two cases. Our Eq. 8 is in fact a matrix equation in spin space, and the associated transfer matrix Eq. 15 is off-diagonal on spin-indices. The partially diagonalized transfer matrix Eq. 19 is defined in the eigenbasis of the helicity operator Σ_L. This set of helical eigenbasis render the non-trivial $\mathbb{Z}_2$ topological properties.

Recently, a paper[54] considered the 3D Hofstadter problem which corresponds to a tilted magnetic field in the cubic lattice with both the nearest and next nearest neighbor hopping. When the flux of each plaquette equals π, time-reversal symmetry is restored. The reduced 1D Aubry-Andre-Harper model belongs to the BDI class[53] and the bulk spectra show Weyl points. Again the flux in this model is complex, and the realized time-reversal symmetry satisfies $T^2 = 1$; while, in our case the time-reversal symmetry satisfies $T^2 = -1$ because of the Kramers degeneracy based on the SU(2) structure. In other words, the time-reversal symmetry in our case is in in the symplectic class; while, it is in the orthogonal class in Ref. 54.

Next we discuss possible experimental realizations of the 3D SU(2) Hofstadter problem. In Refs. 32 and 33, the 3D SU(2) Landau level problems in the continuum have been proposed to be realized in strained semiconductor systems. Nevertheless, as in the case of the U(1) Hofstadter problem, the characteristic length scale of Landau level states is too long compared with the lattice constant and thus the lattice effect can be neglected. The recent development of ultra-cold atom physics provides a promising opportunity to realize the SU(2) Hofstadter problem. Based on the available experimental techniques, such as laser assistant tunneling and shaken lattices, which realized the U(1) Hofstadter problem[40–43], it is natural to expect that the 3D SU(2) Hofstadter problem can also be studied experimentally in the near future. Basically, these techniques need to be extended to spin-dependent hopping or shaking. For a given direction, the associated spin eigenstates are addressed oppositely, such that they acquire opposite phases maintaining time-reversal symmetry. In principle, different spin eigenstates correspond to different internal states of atoms, which have different responses to external lasers, and thus the above spin-dependent manipulations can be realized. The key difficulty is that spin eigen-directions are orthogonal along x and y-bonds due to their non-Abelian nature. These could be realized by different sets of laser beams that control hoppings along the x and y directions separately, and their effects could be superposed together. Along each direction, the spin eigenstates are

chosen according to orthogonal Pauli matrices, respectively. Nevertheless careful designs are still needed to achieve the desired SU(2) Hofstadter Hamiltonian.

VI. CONCLUSIONS

In summary, we have constructed the time-reversal invariant 3D Hofstadter problem based on the 3D SU(2) Landau levels in the Landau-type gauge. This lattice model provides an $SU(2)$ generalization of the usual 2D Hofstadter problem in a magnetic field. For each pair of in plane momenta (k_x, k_y), this system is reduced to 1D described by a generalized $SU(2)$ Harper equation with a helicity structure.

Different from its continuum version, this lattice system possesses 3D translation symmetry as characterized by the periodic spin-dependent potential in the $SU(2)$ Harper equation. Hence, quantitative analysis of the nontrivial $\mathbb{Z}_2$ band topology is performed. In the energy spectra studied in this paper, boundary states with opposite lattice helicity structures are spatially separated at different boundaries; $\mathbb{Z}_2$ non-trivial helical boundary Fermi surface are found and consistent with the $\mathbb{Z}_2$ bulk band topology analyzed based on the parity eigenvalues of the bulk wave functions. The transition of the band topology from a weak topological insulator to a strong one is also investigated.

ACKNOWLEDGMENTS

Y. L. thanks D. Arovas, T. L. Ho, W. Ketterle, and C. Wu for helpful discussions. Y. L. acknowledges the support at the Princeton Center for Theoretical Science. Y. L. also thanks T. L. Ho for his hospitality.

[1] X.-L. Qi and S.-C. Zhang, Physics Today **63**, 33 (2010).
[2] X.-L. Qi and S.-C. Zhang, Rev. Mod. Phys. **83**, 1057 (2011).
[3] M. Z. Hasan and C. L. Kane, Rev. Mod. Phys. **82**, 3045 (2010).
[4] K. Klitzing, G. Dorda, and M. Pepper, Phys. Rev. Lett. **45**, 494 (1980).
[5] D. J. Thouless, M. Kohmoto, M. P. Nightingale, and M. den Nijs, Phys. Rev. Lett. **49**, 405 (1982).
[6] B. I. Halperin, Phys. Rev. B **25**, 2185 (1982).
[7] M. Kohmoto, Ann. Phys. **160**, 343 (1985).
[8] F. D. M. Haldane, Phys. Rev. Lett. **61**, 2015 (1988).
[9] C. L. Kane and E. J. Mele, Phys. Rev. Lett. **95**, 226801 (2005).
[10] B. A. Bernevig and S. C. Zhang, Phys. Rev. Lett. **96**, 106802 (2006).
[11] B. A. Bernevig, T. L. Hughes, and S. C. Zhang, Science **314**, 1757 (2006).
[12] X.-L. Qi, T. L. Hughes, and S.-C. Zhang, Phys. Rev. B **78**, 195424 (2008).
[13] L. Fu and C. L. Kane, Phys. Rev. B **76**, 045302 (2007).
[14] J. E. Moore and L. Balents, Phys. Rev. B **75**, 121306 (2007).
[15] R. Roy, New J. Phys. **12**, 065009 (2010).
[16] M. König, S. Wiedmann, C. Brüne, A. Roth, H. Buhmann, L. W. Molenkamp, X.-L. Qi, and S.-C. Zhang, Science **318**, 766 (2007).
[17] D. Hsieh, D. Qian, L. Wray, Y. Xia, Y. Hor, R. Cava, and M. Hasan, Nature **452**, 970 (2008).
[18] H. Zhang, C. Liu, X. Qi, X. Dai, Z. Fang, and S. Zhang, Nature Phys. **5**, 438 (2009).
[19] Y. Xia, D. Qian, D. Hsieh, L. Wray, A. Pal, H. Lin, A. Bansil, D. Grauer, Y. S. Hor, R. J. Cava, and M. Z. Hasan, Nature Physics **5**, 398 (2009).
[20] Y. L. Chen, J. G. Analytis, J.-H. Chu, Z. K. Liu, S.-K. Mo, X. L. Qi, H. J. Zhang, D. H. Lu, X. Dai, Z. Fang, S. C. Zhang, I. R. Fisher, Z. Hussain, and Z.-X. Shen, Science **325**, 178 (2009), http://www.sciencemag.org/content/325/5937/178.full.pdf.
[21] D.-X. Qu, Y. S. Hor, J. Xiong, R. J. Cava, and N. P. Ong, Science **329**, 821 (2010), http://www.sciencemag.org/content/329/5993/821.full.pdf.
[22] R. Laughlin, Phys. Rev. Lett. **50**, 1395 (1983).
[23] F. Haldane, Phys. Rev. Lett. **51**, 605 (1983).
[24] S. Zhang and J. Hu, Science **294**, 823 (2001).
[25] D. Karabali and V. Nair, Nucl. Phys. B **641**, 533 (2002).
[26] H. Elvang and J. Polchinski, Comptes Rendus Physique **4**, 405 (2003).
[27] B. A. Bernevig, J. Hu, N. Toumbas, and S. C. Zhang, Phys. Rev. Lett. **91**, 236803 (2003).
[28] K. Hasebe, Symmetry, Integrability and Geometry: Methods and Applications **6** (2010).
[29] J. M. Edge, J. Tworzydło, and C. W. J. Beenakker, Phys. Rev. Lett. **109**, 135701 (2012).
[30] K. Hasebe, Nuclear Physics B **886**, 952 (2014), arXiv:1403.5066 [hep-th].
[31] K. Hasebe, Nuclear Physics B **886**, 681 (2014), arXiv:1403.7816 [cond-mat.str-el].
[32] Y. Li and C. Wu, Phys. Rev. Lett. **110**, 216802 (2013).
[33] Y. Li, S.-C. Zhang, and C. Wu, Phys. Rev. Lett. **111**, 186803 (2013).
[34] S. M. Haaker, F. A. Bais, and K. Schoutens, Phys. Rev. A **89**, 032105 (2014).
[35] Y. Li, K. Intriligator, Y. Yu, and C. Wu, Phys. Rev. B **85**, 085132 (2012).
[36] Y. Li, X. Zhou, and C. Wu, Phys. Rev. B **85**, 125122 (2012).
[37] D. R. Hofstadter, Phys. Rev. B **14**, 2239 (1976).
[38] Y. Hatsugai, Phys. Rev. Lett. **71**, 3697 (1993).
[39] Y. Hatsugai, Phys. Rev. B **48**, 11851 (1993).
[40] H. Miyake, G. A. Siviloglou, C. J. Kennedy, W. C. Burton, and W. Ketterle, Phys. Rev. Lett. **111**, 185302 (2013).
[41] M. Aidelsburger, M. Atala, M. Lohse, J. T. Barreiro, B. Paredes, and I. Bloch, Phys. Rev. Lett. **111**, 185301 (2013).
[42] A. Celi, P. Massignan, J. Ruseckas, N. Goldman, I. B. Spielman, G. Juzeliunas, and M. Lewenstein, Phys. Rev. Lett. **112**, 043001 (2014).

[43] D. Jaksch and P. Zoller, New Journal of Physics **5**, 56 (2003), quant-ph/0304038.
[44] K. Osterloh, M. Baig, L. Santos, P. Zoller, and M. Lewenstein, Phys. Rev. Lett. **95**, 010403 (2005).
[45] T. Kimura, arXiv:1210.6355 (2012), arXiv:1210.6355 [cond-mat.mes-hall].
[46] M. S. Scheurer, S. Rachel, and P. P. Orth, arXiv preprint arXiv:1406.7396 (2014).
[47] C. Wu, B. Bernevig, and S. Zhang, Phys. Rev. Lett. **96**, 106401 (2006).
[48] B. I. Halperin, Japanese Journal of Applied Physics **26**, 1913 (1987).
[49] G. Montambaux and M. Kohmoto, Phys. Rev. B **41**, 11417 (1990).
[50] M. Kohmoto, B. I. Halperin, and Y.-S. Wu, Phys. Rev. B **45**, 13488 (1992).
[51] M. Koshino, H. Aoki, K. Kuroki, S. Kagoshima, and T. Osada, Phys. Rev. Lett. **86**, 1062 (2001).
[52] M. Koshino and H. Aoki, Phys. Rev. B **69**, 081303 (2004).
[53] S. Ryu, A. Schnyder, A. Furusaki, and A. Ludwig, New J. Phys. **12**, 065010 (2010).
[54] S. Ganeshan and S. Das Sarma, Phys. Rev. B **91**, 125438 (2015).